

A Solidification Diagram for Ni-Cr-Mo-Gd Alloys Estimated by Quantitative Microstructural Characterization and Thermal Analysis

D.F. SUSAN, C.V. ROBINO, M.J. MINICOZZI, and J.N. DuPONT

A γ -Gd solidification diagram is proposed as an aid to understanding solidification behavior of Ni-Cr-Mo-Gd alloys. In this system, the Ni-Cr-Mo solid solution γ primary austenite phase is treated as the “solvent” and Gd is treated as the solute. The proposed diagram, which has features characteristic of a binary “eutectic” system, was constructed by combining differential thermal analysis and quantitative microstructural analysis data. As a result of the partially divorced solidification microstructure in the ingots studied, determination of the fraction eutectic, and hence the eutectic composition, requires the use of advanced image analysis techniques. The diagram displays a number of features that are very similar to the Ni-Gd binary system and can be used to assess the influence of the Gd concentration on solidification behavior.

I. INTRODUCTION

SAFE transportation and long-term storage of spent nuclear fuel requires development of an alloy with high thermal neutron cross section for construction of the casks used to transport and store the spent fuel. Due to the relatively large amount of material needed for this application and fabrication requirements of the casks, the alloy should exhibit good high-temperature ductility (so that it can be prepared into standard product forms using conventional ingot metallurgy techniques) and possess a narrow solidification temperature range (so that it can be fabricated using fusion welding processes without the risk of solidification cracking). Recent research in this area^[1,2] has shown that the addition of Gd, a strong neutron absorbing element, to a commercial UNS N06455 Ni-based austenitic (Ni-Cr-Mo) alloy matrix can meet these requirements.

As shown in Figure 1 and described in detail elsewhere,^[2] the as-solidified Gd-enriched N06455 alloys exhibit a two-phase microstructure consisting of primary γ -austenite dendrites and an interdendritic γ/GdNi_5 “eutectic”-type constituent. Quantitative compositional measurements made across the γ dendritic substructure using electron microprobe demonstrated that there was no detectable solubility of Gd in the austenite matrix (less than the 0.1 wt pct lower resolution limit of EPMA).^[2] This indicates that Gd segregates aggressively to the liquid phase during solidification, and essentially all the Gd resides within the GdNi_5 gadolinide phase. Thus, the solidification behavior and corresponding microstructure are analogous to a simple binary system. Solidification begins with a primary $L \rightarrow \gamma$ stage in which the liquid becomes enriched in Gd. This process continues until the Gd concentration in the liquid is enriched to the $L \rightarrow \gamma + \text{GdNi}_5$ eutectic composition, at which point solidification

terminates by the formation of the interdendritic γ/GdNi_5 constituent.

The development of these alloys is in its early stages and, as a result, little data are available for the development of tools to aid in understanding microstructural control, particularly in fusion welds. In view of this, it is desirable to summarize any available information for use in future alloy optimization and processing research. This article describes the assembly of differential thermal analysis and microstructural characterization data into a simple binary γ -Gd solidification diagram. The proposed diagram is analogous to a simple eutectic binary phase diagram and may be helpful in future alloy development activities.

II. EXPERIMENTAL PROCEDURES

Two sets of N06455-Gd alloys were analyzed and their compositions are shown in Tables I and II. The alloys were produced by vacuum induction melting of elemental components and casting into steel molds of approximately $5 \times 5 \times 15$ cm (Table I) or $10 \times 10 \times 30$ cm (Table II). The alloys shown in Table I were used for differential thermal analysis (DTA) in order to determine liquidus and eutectic temperatures, while the alloys in Table II were used for microstructural characterization of the as-cast microstructure. In each case, the sets contain alloys from ~ 0.5 to 2.45 to 2.80 wt pct Gd in approximately 0.5 wt pct Gd increments. The DTA was conducted on a Netzsch STA 409 unit (Netzsch Instruments, Burlington, MA) using samples weighing 250 to 500 mg. Alumina was used as the reference material. The DTA samples were packed in alumina powder inside alumina crucibles, and the scans were conducted in an atmosphere of flowing argon. The samples were heated and cooled through the solidification temperature range at a rate of $10^\circ\text{C}/\text{min}$, and reaction temperatures were taken as deviations from the local baseline.

Metallographic samples of the as-cast ingots in Table II were prepared in thermosetting epoxy mounts and were ground and polished using standard metallographic procedures, with the final step consisting of vibratory polishing using $0.05\text{-}\mu\text{m}$ colloidal silica. Samples were tint etched for analysis using Beraha's 7A solution.^[3] This etchant only

D.F. SUSAN, Senior Member of Technical Staff, and C.V. ROBINO, Distinguished Member of Technical Staff, are with the Joining and Coating Department, Sandia National Laboratories, Albuquerque, NM 87185. Contact e-mail: dfsusan@sandia.gov M.J. MINICOZZI, formerly Graduate Student, is with PECO/Exelon Corp., Limerick Nuclear Plant, Pottstown, PA. J.N. DuPONT, Associate Professor, is with the Department of Materials Science & Engineering, Lehigh University, Bethlehem, PA 18015.

Manuscript submitted October 25, 2005.

colors the GdNi_5 phase and does not appreciably attack the γ/GdNi_5 interfaces. Therefore, the optical contrast was suitable for image analysis without introducing errors commonly found with chemical etchants that attack interphase boundaries. Image analysis was performed on a Clemex Vision PE system. Because of the relatively high resolution required and in order to maximize statistical validity of the volume fraction measurements, individual analyses were performed on three or four mosaic (sometimes called “montage”) images for each condition. Each mosaic image consisted of 12 combined images (each image collected at 500 times magnification) so a total of 36 to 48 images were analyzed for each alloy. This approach allowed for eutectic spacing measurement at high resolution and simultaneous phase fraction measurements of large areas on the same mosaic image. Advanced image

analysis correction procedures were used to account for the portion of the eutectic γ that grows on the primary γ dendrites. This was accomplished by using the methods described by Dutta and co-workers.^[5–8] Since it was observed that eutectic microstructures for all compositions were partly divorced in character^[4] (Figure 1), additional modifications were applied to the Dutta *et al.* method to account for the partly divorced character of the eutectic regions. As a verification of this volume fraction correction method, higher magnification images were also obtained with scanning electron microscopy (SEM). Images for this analysis were obtained only from isolated regions where coupled growth of the eutectic constituents was dominant. The images were taken at 5 kV in backscattered electron imaging mode on a Zeiss Supra 55VP scanning electron microscope.

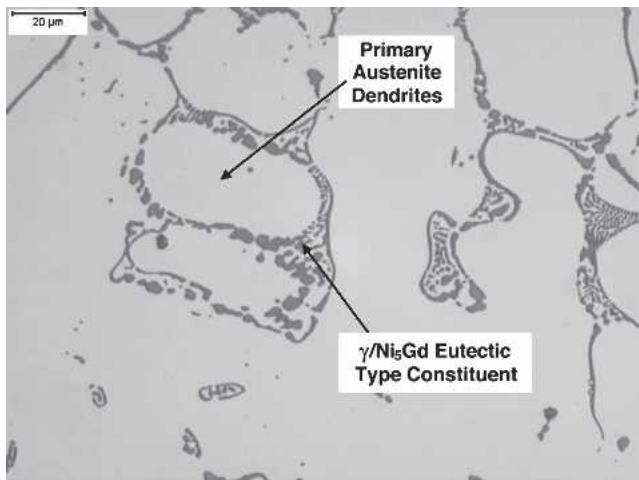


Fig. 1—Light optical photomicrograph of Ni-Cr-Mo-Gd alloy with 1.9 wt pct Gd showing primary austenite dendrites and interdendritic γ/GdNi_5 eutectic-type constituent.

III. RESULTS AND DISCUSSION

A. Liquidus Temperatures

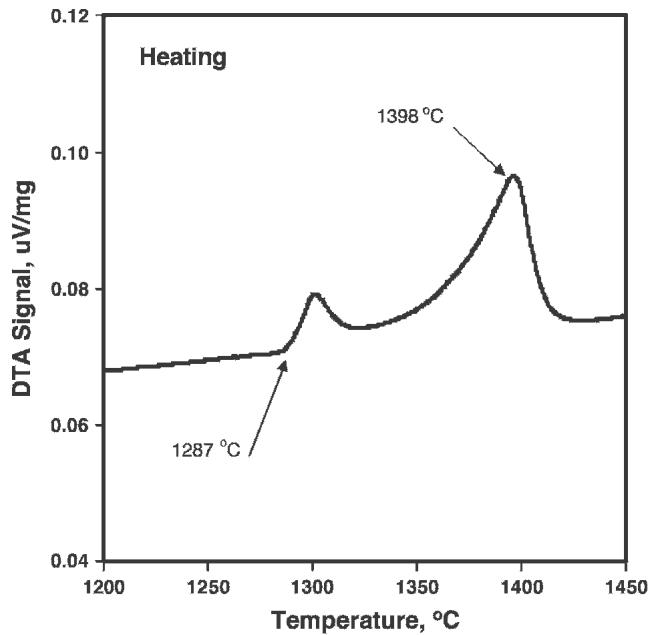
Figure 2 shows typical DTA heating (Figure 2(a)) and cooling (Figure 2(b)) curves. On heating, the γ/GdNi_5 eutectic-type constituent begins to liquate at 1287 °C for this 2.23 wt pct Gd alloy, and the liquidus is reached at 1398 °C. During cooling, the primary γ phase exhibits 64 °C of undercooling before it begins to solidify at 1334 °C, and the γ/GdNi_5 eutectic-type constituent begins to form at 1255 °C. Table III summarizes the DTA heating and cooling data. The average values are reported from two or three tests conducted for each alloy. (The wide variation and large standard deviation values associated with the liquidus temperatures measured on cooling are attributed to undercooling.). The liquidus temperature generally decreases with increasing Gd concentration, while the variation in the eutectic temperature is not as significant. The characteristics of the DTA curves are similar to that which would be expected for a binary eutectic alloy. The initial slope of the

Table I. Measured Compositions of Ni-Gd-Mo-Cr Alloys Used for Differential Thermal Analysis; All Values Shown in Weight Percent

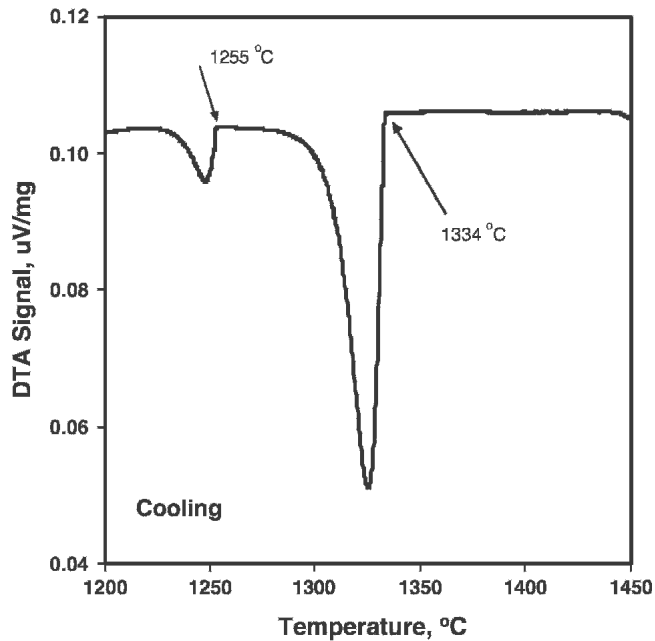
Alloy	Element (Weight Percent)										
	Ni	Mo	Cr	Fe	Gd	P	S	Si	O	N	C
1A	67.69	16.19	15.18	0.05	0.54	<0.001	<0.001	0.13	0.0051	0.0042	0.009
2A	68.53	15.19	14.75	0.05	1.13	<0.001	<0.001	0.13	0.0066	0.0047	0.009
3A	68.83	14.81	14.15	0.06	1.75	<0.001	<0.001	0.14	0.0068	0.0043	0.008
4A	69.34	14.11	13.76	0.07	2.23	<0.001	<0.001	0.15	0.0028	0.0069	0.035
5A	72.6	13.53	13.31	0.09	2.8	<0.001	<0.001	0.15	0.0045	0.0041	0.027

Table II. Measured Compositions of Ni-Gd-Mo-Cr Alloys Used for Microstructural Characterization; All Values Shown in Weight Percent

Alloy	Element (Weight Percent)										
	Ni	Mo	Cr	Fe	Gd	P	S	Si	O	N	C
1B	67.7	15.67	16.00	0.016	0.46	<0.001	<0.001	0.070	0.0044	0.0045	0.0052
2B	67.2	15.53	16.08	0.017	1.01	<0.001	<0.001	0.081	<0.001	0.0044	<0.005
3B	66.9	15.56	15.91	0.015	1.49	<0.001	<0.001	0.070	<0.001	0.0039	0.0064
4B	66.8	15.16	15.95	0.016	1.9	<0.001	<0.001	0.070	0.0021	0.0041	0.0065
5B	66.7	15.12	15.56	0.016	2.45	<0.001	<0.001	0.071	0.0056	0.0043	0.0066



(a)



(b)

Fig. 2—Differential thermal analysis curves for alloy 4A with 2.23 wt pct Gd: (a) heating and (b) cooling.

exothermic peak associated with the eutectic-like reaction (at 1255 °C in Figure 2(b)) is relatively steep and the peak reaches its local minimum at approximately 1250 °C. This implies that the eutectic reaction occurs over a narrow temperature range and, in this respect, is also similar to the invariant eutectic temperature of binary alloys.

B. Constituent Fractions

Table IV summarizes the measured amounts of the GdNi₅ phase within each alloy. Since there is no solubility

Table III. Summary of Liquids and Eutectic Temperatures Measured Using Differential Thermal Analysis

Alloy	Gd Concentration, (Wt Pct)	Heating		Cooling	
		Eutectic (°C)	Liquidus (°C)	Eutectic (°C)	Liquidus (°C)
1A	0.54	1298 ± 2	1413 ± 4	1265 ± 4	1365 ± 14
2A	1.13	1300 ± 1	1410 ± 3	1260 ± 2	1313 ± 4
3A	1.75	1293 ± 1	1397 ± 3	1258 ± 4	1331 ± 20
4A	2.23	1289 ± 1	1397 ± 2	1251 ± 5	1345 ± 28
5A	2.80	1291 ± 2	1392 ± 1	1256 ± 6	1342 ± 16

of Gd in the matrix, the theoretical mass fraction of GdNi₅ in the alloy, $m_{GdNi_5}^A$, is given simply by

$$m_{GdNi_5}^A = C_{Gd}^A / C_{Gd}^{GdNi_5} \quad [1]$$

where C_{Gd}^A is the nominal Gd concentration in the alloy and $C_{Gd}^{GdNi_5}$ is the Gd concentration in the GdNi₅ phase. The composition of the GdNi₅-type phase in these alloys has been measured to be 63Ni-2Cr-35Gd (in wt pct).^[2] The room-temperature density of GdNi₅ was estimated from knowledge of its crystal structure and lattice parameter to be 9.0 Mg/m³, while the room-temperature density reported for the austenitic N06455 matrix is 8.6 Mg/m³. Using these densities, the theoretical mass fraction values estimated with Eq. [1] can be converted to volume fractions. Figure 3 compares the measured and calculated amounts of GdNi₅ phase (in volume percentages). The very good agreement between measured and calculated values supports the observation that all the Gd resides within the GdNi₅ phase and improves confidence in the measured volume fractions.

C. Quantitative Image Analysis Techniques Applied to γ -GdNi₅ Microstructures

In quantitative analysis of eutectic microstructures, a difficulty in measurement arises because some unknown portion of eutectic γ (γ_{eut}) forms on the primary γ dendrites and is indistinguishable from the primary phase. As noted earlier, for the γ /GdNi₅ eutectic, the determination of the volume fraction of eutectic is further complicated by the observation that terminal solidification in these ingots is partially divorced in character. In this article, the term “divorced eutectic” does not imply that the two phases in the eutectic grow separately, *i.e.*, cooperative simultaneous growth *vs* divorced growth (with no exchange of solute between the two solid phases at the solidification front).^[9] Rather, in this study, the definition of divorced eutectic is based solely on morphology; in regions of divorced eutectic, the microstructure is composed of just one layer of GdNi₅ enclosed by γ_{eut} , which had grown directly upon the surfaces of the primary γ dendrites.^[4,10-12] In contrast, regions with well-developed lamellar structures are termed “coupled” or “lamellar” eutectic. In these alloys, the divorced eutectic structure appears mainly in the small spaces between dendrites, while the coupled/lamellar structure is found in larger interdendritic “pockets.” The distinction between the two types of eutectic microstructure is not always well defined, but it becomes important in the

Table IV. Summary of Volume Percentages of GdNi₅ and γ /GdNi₅ Eutectic-Type Constituent within Each Alloy; Eutectic Phase Fractions are Shown for the D-E Method Developed by Dutta *et al.* and the Modified D-E Method Used to Analyze Partly Divorced Eutectic

Alloy	Gd Concentration (Wt Pct)	Pct Vol GdNi ₅	Vol Pct γ /GdNi ₅ Eutectic (D-E Method)	Vol Pct GdNi ₅ within γ /GdNi ₅ Eutectic (D-E Method)	Vol Pct γ /GdNi ₅ Eutectic (Modified D-E Method)	Vol Pct GdNi ₅ within γ /GdNi ₅ Eutectic (Modified D-E Method)
1B	0.46	1.28 ± 0.15	2.87 ± 0.46	44.9 ± 4.10	3.20 ± 0.44	40.1 ± 2.00
2B	1.01	2.71 ± 0.77	6.49 ± 1.80	41.8 ± 0.40	6.65 ± 1.85	40.8 ± 0.24
3B	1.49	3.47 ± 0.43	8.72 ± 0.99	39.8 ± 0.90	8.95 ± 1.03	38.7 ± 0.89
4B	1.90	5.75 ± 0.22	12.78 ± 0.61	45.2 ± 0.60	13.10 ± 0.65	43.9 ± 0.50
5B	2.45	7.23 ± 0.52	16.28 ± 0.87	44.5 ± 2.90	17.41 ± 1.12	41.6 ± 1.90

Overall vol. pct GdNi₅ within eutectic for all photomicrographs from all five alloys = 41.0 ± 1.93 (modified D-E method).

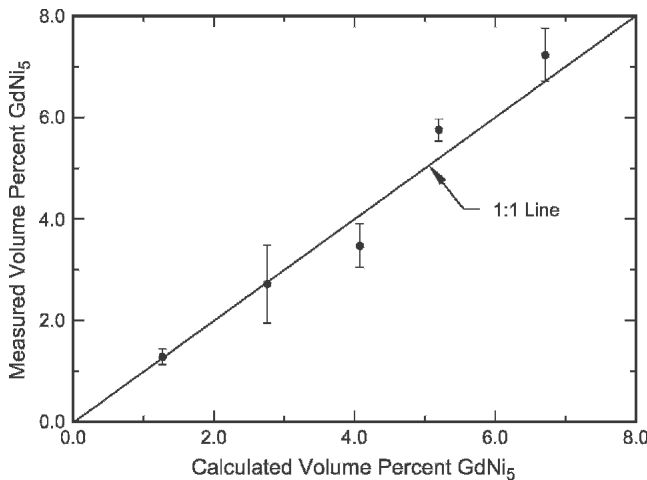


Fig. 3—Comparison between measured and calculated vol pct GdNi₅.

quantitative analysis of phase fractions, as discussed later. The divorced eutectic microstructure is especially prevalent in the lower Gd alloys, where only small amounts of interdendritic liquid remain when the eutectic reaction occurs in the final stages of solidification. In these alloys, few regions are found in the microstructure, which show well-developed lamellar γ /GdNi₅ eutectic. It would be difficult to measure the relative quantities of the eutectic phases (to determine the eutectic composition) in the small coupled growth, lamellar regions of these alloys even with high-magnification SEM. Since an important feature of the solidification diagram is the eutectic composition, a detailed discussion of the means by which the eutectic fraction is determined is warranted.

Figure 4 shows a typical mosaic image and an individual 500 times image from alloy 5B (2.45 wt pct Gd). The image analysis procedures developed by Dutta and co-workers^[5,6,7] and Pompe^[8] were applied to the mosaic images to determine the eutectic fraction in the alloys, taking into account the portion of γ_{eut} that solidifies on the primary γ dendrites. Dutta and co-workers^[5,6,7] and Pompe^[8] used image analysis techniques to estimate the eutectic fraction and the amount of second phase in the eutectic of Al-Si, Al-Fe-Si, and Al-Cu alloys. They applied the image analysis techniques for comparison with published binary phase diagrams and to deter-

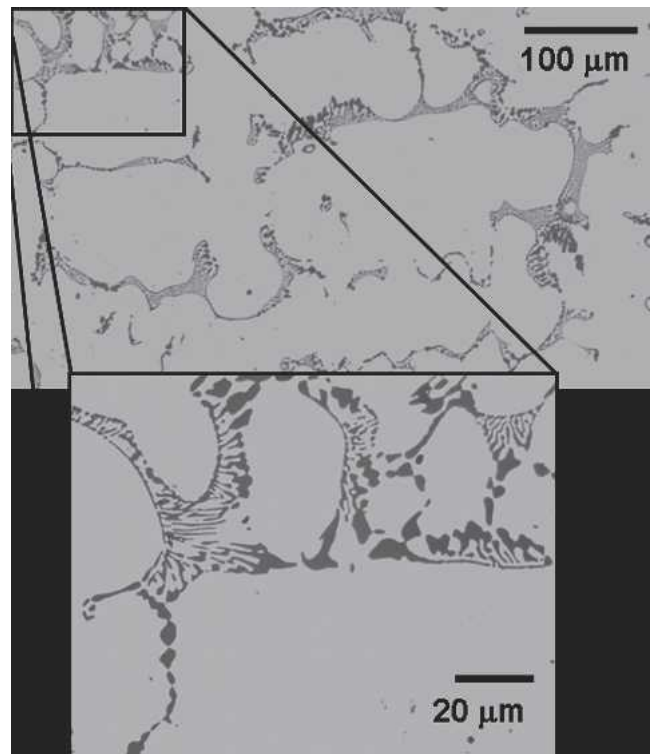


Fig. 4—Mosaic image of alloy 5B consisting of twelve 500 times photomicrographs with one individual photomicrograph enlarged to show the microstructural details.

mine deviations from the phase diagram quantities due to processing conditions, such as varying cooling rates. In the current study, the methods are used to estimate the quantity of eutectic-like constituent in a complex system for which phase diagrams are not available.

The results from one of the methods, the “chord size technique,” are reported here. The first step is to measure the γ /GdNi₅ spacing in the eutectic-like regions. The thresholded images are used with the GdNi₅ phase highlighted. A set of >1000 grid lines is applied to the binary image and the grid line lengths (chord sizes) of the γ regions are measured automatically. This procedure results in several thousand individual chord length measurements. Figure 5 shows histograms of γ chord size data collected

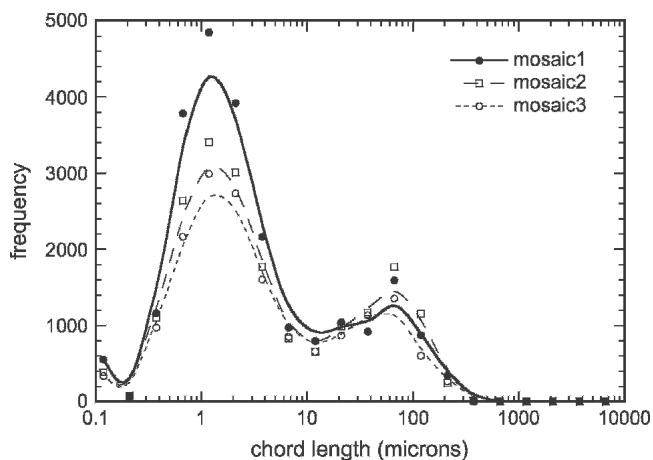


Fig. 5—Frequency distributions of γ chord length from three mosaic images of alloy 5B.

from three mosaic images of alloy 5B. The histograms are produced with equal bin increments on a logarithmic scale. The first peak corresponds to the mean γ spacing in the γ/GdNi_5 eutectic regions, $\bar{L}_{\text{eut}-\gamma}$, and the second peak at approximately $67 \mu\text{m}$ is related to the mean primary γ dendrite size, $\bar{L}_{\text{pri}-\gamma}$.^[5] From Figure 5, the γ_{eut} spacing is taken as $\sim 1.15 \mu\text{m}$. The rather broad distribution in the eutectic spacing is partly due to cross-sectioning effects. The actual distribution of eutectic spacing would be narrower and shifted to shorter lengths if the eutectic colonies were all sectioned perpendicular to their lamellar growth directions. However, it is appropriate to select the peak in the histogram as an estimate of the eutectic spacing, since it will be used to add a region of γ onto the outer edges of the eutectic-like regions. In other words, the same sectioning effects that influence the γ spacing measurements will pertain to the eutectic γ , which grows on the primary dendrites as well. Therefore, the measured thicknesses of this γ layer (if it could be discerned directly from the primary γ) would show a distribution that also depends upon the angle with which the dendrites are sectioned relative to their growth normals.

The next step is to perform a series of image processing operations to fill in the eutectic-like regions while also adding a layer of γ_{eut} , of thickness $\bar{L}_{\text{eut}-\gamma}/2$, at the eutectic region/primary γ interfaces. A number of dilations, D , are applied to the binary image followed by a number of erosions, E , such that

$$D - E = \frac{\bar{L}_{\text{eut}-\gamma}}{2L_{\text{pix}}} \quad [2]$$

where L_{pix} is the size of each pixel in the image. The procedure for determining the correct number of dilations and erosions and other details of the image processing procedure are given elsewhere.^[5,8] At this point, the same thickness of γ_{eut} is assumed to form on the primary γ in all eutectic regions of the microstructure, including areas of divorced eutectic. A portion of a processed image is shown in Figure 6.

Finally, using images such as Figure 6, the volume of GdNi_5 is compared to the volume of the eutectic mixture to obtain the results listed in Table IV (dilation-erosion

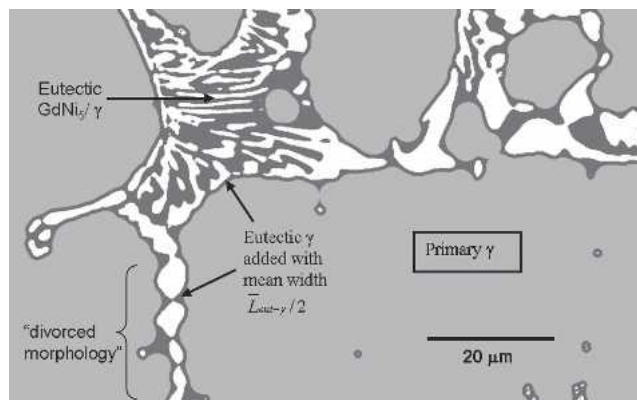


Fig. 6—Processed optical photomicrograph of γ eutectic-type colony showing primary γ regions, eutectic mixture of GdNi_5/γ , and areas of eutectic γ that crystallized over the primary γ phase. The image corresponds to the enlarged region in Fig. 4. A divorced morphology region is indicated in the lower left part of the photomicrograph.

method). The data in Table IV indicate that the amount of γ/GdNi_5 eutectic-type constituent increases with increasing nominal Gd concentration, while the fraction of GdNi_5 phase within the eutectic constituent is relatively insensitive to the nominal Gd concentration. This behavior is similar to that found in a binary eutectic system. Note that the error terms reported in Table IV are standard deviations obtained from the data collected from three or four mosaic images. Therefore, they represent a measure of the microstructural inhomogeneity within the samples and do not represent experimental errors in the image analysis technique (such as pixel resolution, sample preparation, or thresholding errors). In addition, the scatter in the volume percent GdNi_5 within γ/GdNi_5 eutectic (columns 5 and 7 in Table IV) is due to differences in the *distribution of GdNi_5 within the eutectic* due to the partially divorced microstructure in the eutectic regions. This effect is discussed in Section D.

D. Partly Divorced Morphology and Cross-Sectioning Effects

An apparent difference between the Al alloy eutectics studied by Dutta and co-workers^[5,6,7] and Pompe^[8] and the γ/GdNi_5 morphology in the current study is the regions of divorced eutectic morphology (indicated in Figure 6). These locations, which are between dendrites, contain essentially a single layer of GdNi_5 surrounded by γ_{eut} . A complicating factor arises because the thickness of the GdNi_5 phase in most of these locations differs from the lamellar thickness of GdNi_5 found in the coupled growth regions. The divorced parts of the microstructure, therefore, clearly show a different $\gamma_{\text{eut}}/\text{GdNi}_5$ ratio compared to the coupled, lamellar regions after the chord-size image analysis technique is applied (Figure 6). This effect may cause an overestimation of the ratio of GdNi_5 to γ_{eut} shown in Table IV (D-E method), especially for alloys with appreciable amounts of divorced morphology. Note that the different ratios of $\gamma_{\text{eut}}/\text{GdNi}_5$ shown in the divorced region of Figure 6 could also be caused by deviations from true invariant eutectic behavior in this multicomponent alloy.

The relative phase fractions within the eutectic are determined by the maximum solubility of the solute in each phase and the eutectic composition. These values are constant for a simple binary eutectic system, and the relative phase fractions within the eutectic are therefore constant. However, the maximum solubility and eutectic compositions can be temperature dependent in ternary and higher order systems and can therefore vary during the eutectic reaction. This will cause the relative fractions of phases within the eutectic to vary as the eutectic constituent forms at the terminal stages of solidification. In the γ -Gd alloys considered here, there is no solubility of Gd in γ , and the GdNi_5 phase appears to form over a small temperature range (Figure 2(b)) as a line compound with constant Gd concentration. Thus, any potential variation in the relative phase fractions could be caused by possible variations within the eutectic composition. However, it is more likely that the effects shown in the divorced regions are caused simply by adjustments of the $\gamma_{\text{eut}}/\text{GdNi}_5$ spacing. The local conditions of heat flow and mass flow in the liquid between closely approaching dendrites result in a thicker single layer of GdNi_5 and, presumably, a corresponding thicker surrounding layer of γ_{eut} to maintain the eutectic composition. In the larger pockets of interdendritic liquid (coupled growth regions), the eutectic phases adopt a different spacing compared to the divorced regions. With this hypothesis, a second semiautomatic image analysis procedure was developed to reconstruct the γ_{eut} layer surrounding the GdNi_5 in the divorced regions.

Figures 7(a) and (b) show a mosaic image and an individual photomicrograph with the divorced regions highlighted. The reconstructed γ_{eut} layer surrounding the GdNi_5 phase is thicker than the γ_{eut} layer in the coupled, lamellar eutectic regions (Figure 7(b)). The thicker γ_{eut} layer serves to approximately maintain the eutectic composition discussed in Section C. The procedure for delineating the divorced regions involves first constructing the γ_{eut} areas using, for example, the chord length/dilation/erosion technique described earlier (Figure 6). In the second step, image processing is performed, which consists mainly of a series of erosions applied to the γ_{eut} phase. Since the divorced regions of γ_{eut} are generally thinner than the interdendritic pockets, they will be eroded away first. A judgment is necessary, however, to determine the exact boundary between divorced and coupled eutectic regions. In general, regions with a single layer of GdNi_5 , which also had appreciable length, were considered divorced regions (Figure 7(a)). In addition, isolated islands of GdNi_5 were also treated as divorced eutectic, although some of these could be caused by partial sectioning of larger structures. The third step is to measure the average thickness of the GdNi_5 in the divorced regions (average $\sim 2.5 \mu\text{m}$ for alloy 5B). Finally, a layer of γ_{eut} is added to the outside of the GdNi_5 in a similar manner as described previously, with the appropriate thickness to maintain the overall eutectic composition. The result is a somewhat thicker layer of γ_{eut} surrounding the GdNi_5 in the divorced regions. This procedure serves to maintain the eutectic composition on a local scale throughout the microstructure. Perhaps more importantly, it serves to further reconstruct and visualize the liquid phase that was present at the initiation of terminal solidification and illustrates the fact that eutectic solidifica-

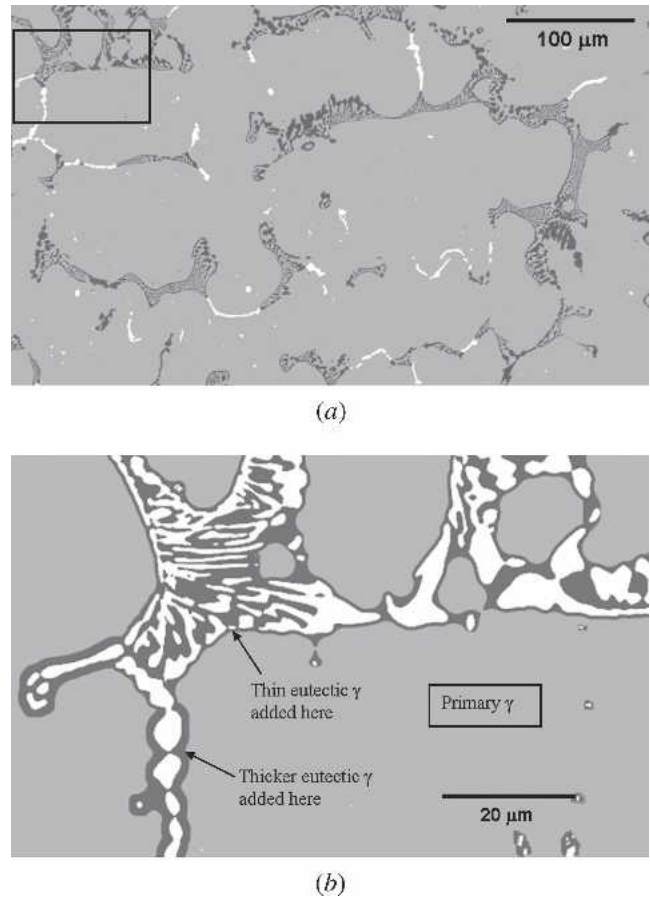


Fig. 7—(a) Mosaic image of alloy 5B after image processing with the regions of divorced eutectic highlighted. (b) Processed optical photomicrograph of alloy 5B microstructure showing primary γ regions, eutectic mixture of GdNi_5/γ , and areas of eutectic γ that crystallized over the primary γ phase. The eutectic γ region surrounding the “divorced” region has been changed to maintain the overall eutectic composition.

tion need not proceed with uniform phase thicknesses in all areas. The image analysis method can be used in any eutectic alloy that shows regions of differing morphology caused by changes in local solidification conditions. Note that the actual thickness of the γ_{eut} phase probably shows a more gradual change in thickness between regions of “divorced” and “coupled lamellar” growth. After application of this second image analysis technique, the resultant eutectic phase fractions are listed in the final two columns of Table IV. The overall volume percentage of GdNi_5 within the eutectic for all alloys is found to be 41.0 ± 1.93 pct. This adjusted phase fraction is also used in construction of the solidification diagram discussed later.

A slight overestimation of the $\text{GdNi}_5/\gamma_{\text{eut}}$ ratio would also be obtained if cross-sectioning effects are considered. The effects of cross sectioning can be seen in Figures 1, 4, 6, and 7, where the thicknesses of the GdNi_5 and γ lamellae change along their lengths within the interdendritic regions. In general, the true thicknesses of the lamellae will be measured when the layers are sectioned perpendicular to their growth direction. The cross-sectioning effects are accounted for, however, by measuring the distribution of the γ_{eut} chord lengths (Figure 5) and using the peak in the histogram to add a layer of γ_{eut} to the eutectic regions.

Also, the dilation and erosion procedures fill in relatively large areas of γ_{eut} within the interdendritic pockets while simultaneously adding a γ_{eut} layer to the outside of the eutectic regions. The dilation/erosion procedure does not add the correct amount of γ_{eut} in the divorced regions, however, if the GdNi_5 thickness is different than in the coupled/lamellar regions. The differences in phase thickness in the divorced regions could be due to adjustments during eutectic growth or due to cross-sectioning effects. The modified procedure described previously is an attempt to adjust the reconstructed eutectic on a local scale within the areas of divorced eutectic and successfully accounts for both cross-sectional effects and changes in lamellar spacing (phase thickness).

To model the alloy behavior as a binary system, the eutectic composition can be estimated from knowledge of the average measured value of approximately 41 vol pct GdNi_5 and 59 vol pct γ austenite. With knowledge of the mass fraction of Gd in GdNi_5 , these results were converted to weight percent to give ~ 14.7 wt pct Gd as the eutectic composition in order to construct a binary solidification diagram, as discussed later. As an illustration of the importance of the image analysis correction procedure, the results obtained in the preceding analysis were compared to data obtained if the technique is not used. If the eutectic regions are simply “filled in” (closed GdNi_5 images) without adding a layer of γ_{eut} on the primary dendrites (a common oversight in image analysis of eutectic structures), the proportion of GdNi_5 in the eutectic is found to vary from 58 to 65 vol pct with an average value of 60.9 ± 2.64 vol pct. This value of GdNi_5 eutectic fraction represents a large error compared to the 41 vol pct GdNi_5 measured in the eutectic if the correction procedure is applied.

As a verification of the volume fraction correction method, higher magnification images containing only eutectic constituents were also obtained using SEM. This procedure can only be applied to the high Gd alloys that contain isolated regions of predominantly coupled growth and that are large enough for accurate quantitative measurement at high magnification. Photomicrographs for this analysis were taken in selected areas of alloy 5B. Figure 8(a) shows a typical backscatter electron (BSE) photomicrograph obtained at 5 kV accelerating voltage. A total of seven images from alloy 5B were analyzed to determine the volume fractions of the eutectic constituents. Figure 8(b) shows a binary digitized image with the GdNi_5 phase highlighted. The measured volume percent of GdNi_5 within the eutectic regions was 40 ± 0.8 vol pct. This value agrees very well with the optical microscopy/image analysis technique (41 ± 1.9 vol pct) described previously.

E. Solidification Diagram

The N06455-Gd alloys exhibit a solidification sequence and corresponding solidification microstructure that is reminiscent of a simple binary eutectic system. In this case, the “solvent” can be represented by the Ni-Cr-Mo solid solution γ -austenite phase and Gd can be treated as the solute element. The similarity of this γ -Gd binary system to a binary eutectic system is readily evident in several ways, including the following: the as-solidified microstructure consisting of primary γ dendrites surrounded by an inter-

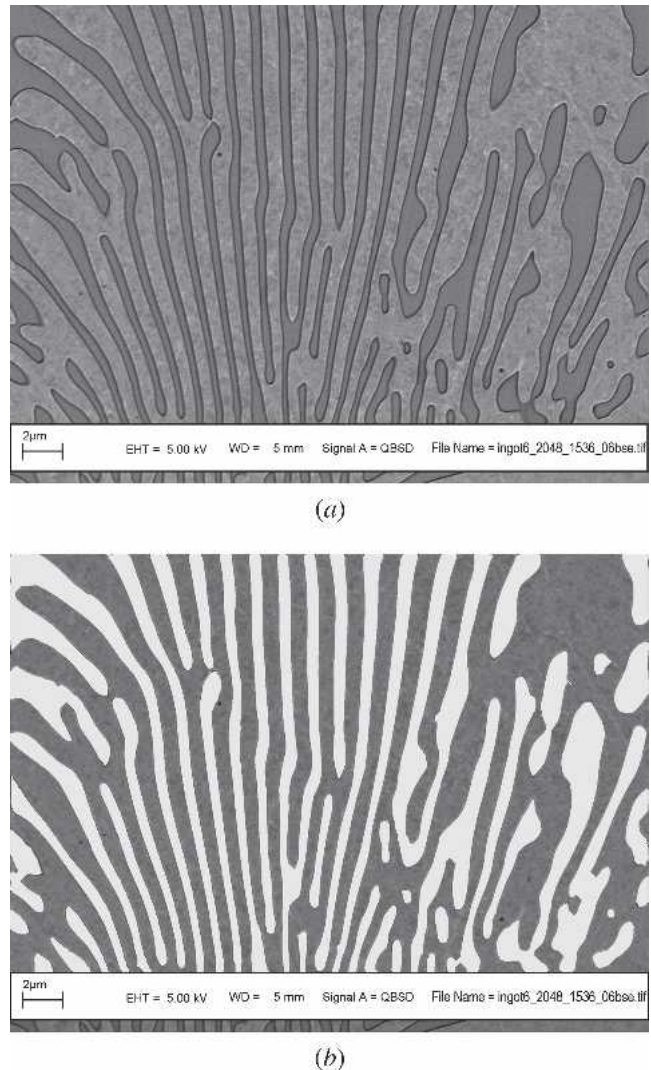


Fig. 8—A backscatter electron photomicrograph and a binary digitized image of isolated eutectic-type region in alloy 5B.

dendritic eutectic-type constituent in which the secondary phase in the eutectic is solute rich; the amount of eutectic-type constituent increasing with increasing solute content; and the proportional amount of each phase within the eutectic being relatively insensitive to nominal solute content. Also note that the eutectic temperature is not strongly dependent on the nominal Gd concentration. With these similarities in mind, the image analysis and thermal analysis data can be combined to develop a binary γ -Gd solidification diagram. The term “solidification” diagram is used here in preference to “phase” diagram since the information used to construct the diagram was acquired from DTA solidification scans and characterization of as-solidified microstructures. As such, the diagram cannot be considered a phase diagram but rather pertains mainly to understanding solidification behavior.

The solidification diagram is shown in Figure 9. The data for the liquidus line were acquired from the heating DTA scans and the nominal Gd concentrations along with the liquidus temperature for a nominal UNS N06455 alloy (1427 °C). The eutectic line is plotted at a constant value of 1258 °C, which is the average eutectic temperature from

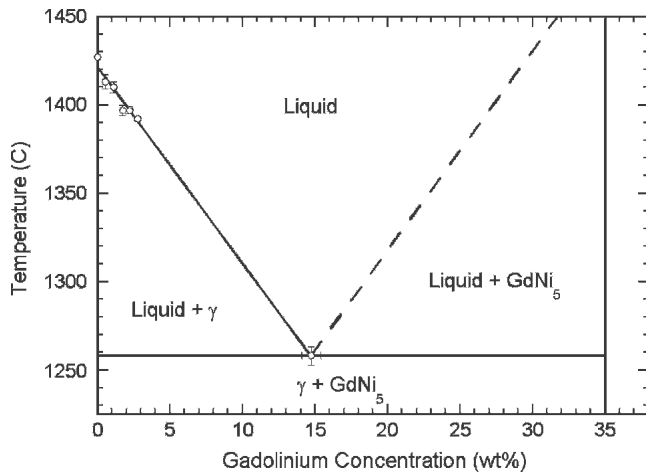


Fig. 9—Binary γ -Gd solidification diagram. The liquidus temperatures were determined on heating and the eutectic temperature was determined on cooling at 10 °C/min. The eutectic composition was estimated by image analysis techniques.

all the alloys used for the DTA cooling scans. As previously discussed,^[13,14] the solidification temperature range of fusion welds is best represented by the separation between the on-heating liquidus temperature and on-cooling eutectic temperature, because solidification initiates epitaxially at the fusion line without the need for undercooling. Because control and interpretation of weld fusion zone microstructures is a primary concern in the development of these alloys,^[1,2] these reaction temperatures are chosen. The GdNi_5 phase is treated as an intermetallic line compound and is represented by the vertical line at 35 wt pct Gd. The eutectic line would normally extend from the line compound composition to the maximum solubility of the solid solution primary phase. However, since there is no Gd dissolved within the primary γ austenite, the eutectic line extends to 0 wt pct Gd and there is no γ single-phase field on the diagram. The eutectic composition was not determined directly, but can be estimated from knowledge of the composition and volume fraction of the GdNi_5 phase within the eutectic constituent, as described previously. Because there is no solubility of Gd in the austenite, the eutectic composition, C_{Gd}^e , is simply given by

$$C_{\text{Gd}}^e = m_{\text{GdNi}_5}^{f^e} C_{\text{Gd}}^{\text{GdNi}_5} \quad [3]$$

where $m_{\text{GdNi}_5}^{f^e}$ is the mass fraction of GdNi_5 within the eutectic. As shown in Table IV, the volume fraction of GdNi_5 , $v_{\text{GdNi}_5}^{f^e}$, is essentially constant at 0.41 (the average value). Therefore, this value was taken as the eutectic value and was converted to mass fraction by using the phase densities given earlier. Using this mass fraction (0.421 ± 0.0194) along with the GdNi_5 composition of 35 wt pct and Eq. [3] yields a eutectic composition of $14.7(4) \pm 0.68$ wt pct Gd. Finally, the line representing the liquidus in the liquid + γ phase field is a linear fit of all DTA and image analysis measurements.

F. Comparisons with the Ni-Gd Binary System

Given the similarities between the solidification diagram of Figure 9 and a binary system, it is interesting to compare

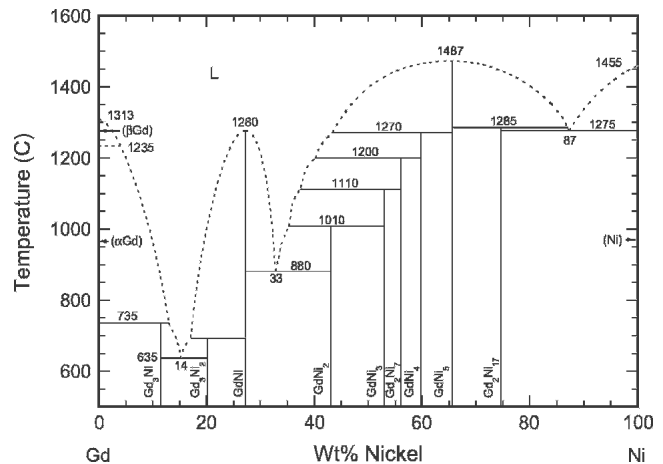


Fig. 10—Binary Ni-Gd phase diagram, adapted from Ref. 15.

the behavior of the Ni-Cr-Mo-Gd alloys with that of the Ni-Gd binary diagram. The phase diagram for the Ni-Gd system^[15] is shown in Figure 10. The diagram indicates a eutectic reaction between $\text{Gd}_2\text{Ni}_{17}$ and Ni and a eutectic composition at 13 wt pct Gd at 1275 °C. GdNi_5 is indicated to form by congruent melting. However, the compound $\text{Gd}_2\text{Ni}_{17}$ has not been observed in any of the extensive characterization work during the development of γ -Gd alloys.^[1,2] It is possible that $\text{Gd}_2\text{Ni}_{17}$ does not form under the heating and cooling rates of this study and the related studies,^[1,2,13,14] which include much larger ingots, or it is possible that the more complex alloy chemistry in this system suppresses formation of a $\text{Gd}_2\text{Ni}_{17}$ -type compound. In any case, if the $\text{Gd}_2\text{Ni}_{17}$ compound is ignored, a simple eutectic can be assumed between GdNi_5 and Ni. The eutectic composition of 87 wt pct Ni indicates that the proportion of constituents within the eutectic in the binary system is about 37 wt pct gadolinide and 63 wt pct Ni and is similar to the 41 pct gadolinide measured here. The general similarities between the Ni-rich portion of the Ni-Gd system and the γ -Gd solidification diagram lend support for the representation of the behavior of these alloys with a binary diagram. The fact that the eutectic point in the binary system has a Ni-rich composition is also supportive of the composition estimated for the eutectic-like composition in this study. Furthermore, the similarities in the relative locations of the eutectic points in the binary system and binary solidification diagram also give confidence in the image analysis technique used to estimate the eutectic-like reaction in the solidification diagram.

IV. CONCLUSIONS

A binary γ -Gd solidification diagram was developed as an aid to understanding the solidification behavior of Ni-Cr-Mo-Gd alloys. The diagram was developed from DTA experiments and microstructural characterization. To estimate the location of the eutectic point in the binary system model, a quantitative metallographic method was employed, which accounted for the portion of eutectic γ that grows on the primary γ dendrites. To characterize the complex partially divorced morphology of the eutectic, advanced image

analysis techniques were applied to reconstruct the morphology of the interdendritic liquid just prior to terminal solidification. The γ -Gd alloy behavior is similar to a simple binary eutectic in several ways, including the following: the as-solidified microstructure consists of primary γ dendrites surrounded by an interdendritic eutectic-type constituent in which the secondary phase in the eutectic is solute rich, the amount of eutectic-type constituent increases with increasing solute content, and the proportional amount of each phase within the eutectic is relatively insensitive to the nominal solute content. The similarities between the Ni-Gd binary system and the γ -Gd diagram provide confidence in the simplified approach to describing the solidification behavior of Ni-Cr-Mo-Gd alloys and further validate the image analysis techniques used to quantify eutectic microstructures.

ACKNOWLEDGMENTS

The authors thank Arlan Benscoter (Lehigh University) and Alice Kilgo (Sandia) for metallography expertise. Special thanks also to Bonnie McKenzie (Sandia) for SEM analysis and to Dr. Joe Michael for careful review of the manuscript. This work was supported by the United States Department of Energy, Assistant Secretary for Environmental Management, under DOE Idaho Operations Office Contract No. DE-AC07-99ID13727. This work was performed at Lehigh University and Sandia National Laboratories through support from the National Spent Nuclear Fuel Program. Sandia is a multiprogram laboratory operated

by Sandia Corporation, a Lockheed Martin Company, for the United States Department of Energy's National Nuclear Security Administration under Contract No. DE-AC04-94AL85000.

REFERENCES

1. C.V. Robino, J.N. DuPont, R.E. Mizia, J.R. Michael, D.B. Williams, and E. Shaber: *J. Mater. Eng. Performance*, 2003, vol. 12 (2), pp. 206-14.
2. J.N. DuPont, C.V. Robino, J.R. Michael, R.E. Mizia, and D.B. Williams: *Welding J.*, 2004, vol. 83, pp. 319s-29s.
3. E. Beraha: *Pract. Metallogr.*, 1971, vol. 8 (9), pp. 547-50.
4. F.N. Rhines: *Phase Diagrams in Metallurgy*, McGraw-Hill, New York, NY, 1956, pp. 43-44.
5. B. Dutta, O. Pompe, and M. Rettenmayr: *Mater. Sci. Technol.*, 2004, vol. 20, pp. 1011-18.
6. B. Dutta and M. Rettenmayr: *Mater. Sci. Technol.*, 2002, vol. 18, pp. 1428-34.
7. B. Dutta and M. Rettenmayr: *Mater. Sci. Eng., A*, 2000, vol. A283, pp. 218-24.
8. O. Pompe: *Pract. Metallogr.*, 1994, vol. 31 (6), pp. 274-83.
9. *ASM Metals Handbook*, 10th Ed., vol. 9, 2004, *Metallography and Microstructures*, ASM INTERNATIONAL, 2004, Materials Park, OH, pp. 81-84.
10. B. Chalmers: *Principles of Solidification*, John Wiley & Sons, New York, NY, 1964, pp. 218-19.
11. R.E. Reed-Hill and R. Abbaschian: *Physical Metallurgy Principles*, 3rd ed., PWS Publishing Company, Boston, MA, 1994, pp. 464-65.
12. S. Wang, T. Akatsu, Y. Tanabe, and E. Yasuda: *J. Mater. Sci.*, 2000, vol. 35, pp. 2757-61.
13. J.N. DuPont, C.V. Robino, and A.R. Marder: *Welding J.*, 1998, vol. 77, pp. 417s-31s.
14. S.A. David and J.M. Vitek: *Int. Mater. Rev.*, 1989, vol. 34, pp. 213-45.
15. R.P. Elliot: *Constitution of Binary Alloys, First Supplement*, McGraw-Hill, New York, NY, 1965, pp. 467-68.